Received: 23 September 2023 | Accepted: 4 June 2024

DOI: 10.1002/jcp.31340

RESEARCH ARTICLE

Journal of Cellular Physiology WILEY

Quantitative assessment of morphological changes in lipid droplets and lipid–mito interactions with aging in brown adipose

Amber Crabtree[1,2] | Kit Neikirk[1] | Julia A. Pinette[1] | Aaron Whiteside[1] | Bryanna Shao[1] | Jessica Bedenbaugh[1] | Zer Vue[1] | Larry Vang[1] | Han Le[1] | Mert Demirci[3] | Taseer Ahmad[4,5] | Trinity Celeste Owens[1] | Ashton Oliver[1] | Faben Zeleke[1] | Heather K. Beasley[1] | Edgar Garza Lopez[6] | Estevão Scudese[1] | Taylor Rodman[1] | Kinuthia Kabugi[1] | Alice Koh[1] | Suzanne Navarro[1] | Jacob Lam[6] | Ben Kirk[6] | Margaret Mungai[1,6] | Mariya Sweetwyne[7] | Ho-Jin Koh[8] | Elma Zaganjor[1] | Steven M. Damo[9] | Jennifer A. Gaddy[10,11] | Annet Kirabo[4] | Sandra A. Murray[12] | Anthonya Cooper[12] | Clintoria Williams[13] | Melanie R. McReynolds[14,15] | Andrea G. Marshall[1] | Antentor Hinton Jr.[1]

[1]Department of Molecular Physiology and Biophysics, Vanderbilt University, Nashville, Tennessee, USA

[2]The Frist Center for Autism and Innovation, Vanderbilt University, Nashville, Tennessee, USA

[3]Department of Medicine, Division Nephrology and Hypertension, Vanderbilt University Medical Center, Nashville, Tennessee, USA

[4]Department of Medicine, Division of Clinical Pharmacology, Vanderbilt University Medical Center, Nashville, Tennessee, USA

[5]Department of Pharmacology, College of Pharmacy, University of Sargodha, Sargodha, Punjab, Pakistan

[6]Department of Internal Medicine, University of Iowa, Iowa City, Iowa, USA

[7]Department of Laboratory Medicine and Pathology, University of Washington, Seattle, Washington, USA

[8]Department of Biological Sciences, Tennessee State University, Nashville, Tennessee, USA

[9]Department of Life and Physical Sciences, Fisk University, Nashville, Tennessee, USA

[10]Division of Infectious Diseases, Vanderbilt University School of Medicine, Nashville, Tennessee, USA

[11]Tennessee Valley Healthcare Systems, U.S. Department of Veterans Affairs, Nashville, Tennessee, USA

[12]Department of Cell Biology, School of Medicine, University of Pittsburgh, Pittsburgh, Pennsylvania, USA

[13]Department of Neuroscience, Cell Biology and Physiology, Wright State University, Dayton, Ohio, USA

[14]Department of Biochemistry and Molecular Biology, Pennsylvania State University, University Park, Pennsylvania, USA

[15]Huck Institutes of the Life Sciences, Pennsylvania State University, University Park, Pennsylvania, USA

Correspondence
Antentor Hinton Jr., Department of Molecular Physiology and Biophysics, Vanderbilt University, Nashville, TN 37232, USA.
Email: antentor.o.hinton.jr@vanderbilt.edu

Abstract

The physical characteristics of brown adipose tissue (BAT) are defined by the presence of multilocular lipid droplets (LDs) within the brown adipocytes and a high abundance

Kit Neikirk and Julia Pinette are cosecond authors. Andrea G. Marshall and Antentor Hinton Jr. are cosenior authors.

Funding information
UNCF/Bristol-Myers Squibb E.E. Just Faculty Fund; BWF Career Awards at the Scientific Interface Award; BWF Ad-hoc Award; NIH PRIDE Small Research Pilot Subaward to 5R25HL106365-12; Department of Veterans Affairs Office of Research, Grant/Award Number: M.T.S. I01 BX005352; Multidisciplinary Training in Molecular Endocrinology, Grant/Award Number: DK007563; NSF NRT, Grant/Award Number: 19-22697(K.Stassun,PI); NSF BPE, Grant/Award Number: 22-17621(K.Stassun,PI); Chan Zuckerberg Initiative DAF, Grant/Award Numbers: 2022-253529, 2022-253614; NIH, Grant/Award Numbers: K01HL130497, R01HL147818, R03HL155041, R01HL144941, K01AG062757; NSF, Grant/Award Numbers: MCB #2011577I, EES2112556, EES1817282, MCB1955975

of iron-containing mitochondria, which give it its characteristic color. Normal mitochondrial function is, in part, regulated by organelle-to-organelle contacts. For example, the contact sites that mediate mitochondria–LD interactions are thought to have various physiological roles, such as the synthesis and metabolism of lipids. Aging is associated with mitochondrial dysfunction, and previous studies show that there are changes in mitochondrial structure and the proteins that modulate organelle contact sites. However, how mitochondria–LD interactions change with aging has yet to be fully clarified. Therefore, we sought to define age-related changes in LD morphology and mitochondria–lipid interactions in BAT. We examined the three-dimensional morphology of mitochondria and LDs in young (3-month) and aged (2-year) murine BAT using serial block face-scanning electron microscopy and the Amira program for segmentation, analysis, and quantification. Our analyses showed reductions in LD volume, area, and perimeter in aged samples in comparison to young samples. Additionally, we observed changes in LD appearance and type in aged samples compared to young samples. Notably, we found differences in mitochondrial interactions with LDs, which could implicate that these contacts may be important for energetics in aging. Upon further investigation, we also found changes in mitochondrial and cristae structure for the mitochondria interacting with LDs. Overall, these data define the nature of LD morphology and organelle–organelle contacts during aging and provide insight into LD contact site changes that interconnect biogerontology with mitochondrial function, metabolism, and bioactivity in aged BAT.

KEYWORDS
brown adipose tissue (BAT), lipid droplets (LD), lipids, mitochondria, mito–lipid

1 | INTRODUCTION

Mitochondria have numerous indispensable functions, including the maintenance of calcium homeostasis, but they are most often appreciated for their role in energy production (Afzal et al., 2021). Within mitochondrial networks, the function of each mitochondrion is believed to be both tissue and cell-type-dependent (Glancy et al., 2020; Naik et al., 2019). As mitochondrial function is tightly associated with mitochondrial morphology, mitochondrial ultrastructure changes in accordance with the energetic and functional demands of the cell (Brandt et al., 2017; Glancy et al., 2020). Consistent with this specialization, functional and subsequently, morphological, heterogeneity is observed in various tissue and cell types (Jenkins et al., 2024). For example, mitochondria typically display a branched phenotype in the transverse orientation and are located between myofibrils in skeletal muscle due to their high energetic needs; in contrast, cardiac mitochondria demonstrate a compact phenotype (Vue, Neikirk, et al., 2023). Mitochondrial heterogeneity is also observed within each cell and this is somewhat dependent on subcellular localization (e.g., position in intermyofibrillar or subsarcolemmal regions) and their dynamic nature (Glancy et al., 2020; Naik et al., 2019).

Mitochondrial dynamics consist of coordinated cycles of fusion and fission, which provide a means for content mixing, quality control, and the maintenance of healthy mitochondrial networks (Tilokani et al., 2018). In brown adipose tissue (BAT), the reorganization of the mitochondrial ultrastructure works cooperatively with the release of free fatty acids to promote heat production via uncoupled respiration (Gao & Houtkooper, 2014; Wikstrom et al., 2014). Immediately following cold exposure or adrenergic stimulation, mitochondrial fission is promoted, which is essential for BAT thermogenesis (Lee et al., 2019; Wikstrom et al., 2014). Moreover, recent studies demonstrate the role of mitochondrial architecture in maintaining thermogenic capacity and energy homeostasis in BAT (de-Lima-Júnior et al., 2019; Rodríguez-Cuenca et al., 2002; Townsend & Tseng, 2014). During the aging process, a functional decline in BAT is observed and is associated with the onset of metabolic disorders, including type II diabetes (Peres Valgas da Silva et al., 2022; Pfannenberg et al., 2010). Given that altered mitochondrial structure, metabolism, and bioenergetics are associated with insulin resistance and type II diabetes (Rovira-Llopis et al., 2017), the intricate relationship between BAT and mitochondrial structure may offer insight into metabolic pathomechanisms.

Recently, we showed that in murine BAT, aging is associated with a loss of the inner mitochondrial folds, known as cristae, and an increase in mitochondrial volume and matrix (Crabtree et al., 2024). Although a high abundance of mitochondria is a notable characteristic of thermogenic adipose tissue, it is not the only defining

characteristic. Multilocular lipid droplets (LDs), as opposed to the unilocular LDs observed in white adipose tissue, are also a defining feature of thermogenic adipose tissue (Chen et al., 2022). Studies have shown that the composition and distribution of lipids in BAT can alter mitochondrial function and efficiency (Johnson & Stolzing, 2019; Pereira et al., 2022; Yu et al., 2015). Additionally, across aging, BAT has been illustrated to accumulate phospholipids, sphingolipids, and dolichols (Gohlke et al., 2019), which points toward increased LD formation that may be counteracted by mitochondria–LD-mediated lipolysis (Renne & Hariri, 2021; Song, Hogstrand, et al., 2020; Yang et al., 2022).

LDs are considered dynamic organelles that play a role in various cellular pathways (Renne & Hariri, 2021). Mitochondria are known to make contact and associate with LDs and other organelles, allowing for the fine-tuning of vital processes, such as calcium signaling, lipid synthesis, apoptosis, and the formation of autophagosomes (Giacomello & Pellegrini, 2016; Jenkins et al., 2024; Neikirk, Vue, et al., 2023; Yang et al., 2022; Yu et al., 2015). In tissues with a high capacity for oxidative metabolism, mitochondria and LDs show extensive interaction networks. In BAT, mitochondria–LD interactions increase following cold stimulation, presumably to facilitate fatty acid consumption for thermogenesis (Benador et al., 2018; Chen et al., 2022; Cui & Liu, 2020; Yu et al., 2015). These interactions are categorized into either dynamic or stable subgroups according to their interaction strength (Benador et al., 2018; Boutant et al., 2017; Tarnopolsky et al., 2007). Dynamic interactions are those that can be disrupted using high-speed centrifugation, which include peridroplet mitochondria, whereas stable interactions remain undisrupted using high-speed centrifugation and are also known as LD-anchored mitochondria (Chen et al., 2022; Yu et al., 2015). Although our understanding of mitochondria–LD interactions is evolving, changes in organelle contacts that occur with aging remain incompletely understood.

To better examine how the aging process affects LDs and their associations with mitochondria, we utilized murine BAT and serial block-face scanning electron microscopy (SBF-SEM) combined with three-dimensional (3D) reconstruction to quantitatively study these organelle interactions with a relatively high spatial resolution (Courson et al., 2021; Lippens et al., 2019; Marshall et al., 2023). As with many techniques in EM quantification, minor errors may arise due to the manual tracing method and the irregularity in mitochondrial shape. In addition, the fine distance between organelle contacts is a source of potential error with many automated systems (Neikirk, Lopez, et al., 2023). Thus, to ensure the highest accuracy, we employed manual mitochondria and LD contour tracing using previously validated techniques (Garza-Lopez et al., 2022). We hypothesized that mitochondria–lipid interactions and lipid morphology dynamics would change with aging. As the first to study 3D organelle–organelle contacts in adipose tissue across aging, we characterized structural changes that may yield valuable insights into the age-related decline in BAT thermogenic capacity and mitochondrial function.

2 | METHODS

2.1 | Animal housing and care

C57BL/6J male mice were housed at 22°C with ad libitum food and water intake and maintained with alternating 12-h dark/12-h light cycles. Mice were cared for as previously described by Lam et al. (2021). All animal protocols were approved by the University of Iowa Animal Care and Use Committee.

2.2 | SBF-SEM sample preparation

All subsequent preparation and analyses were performed by individuals blinded to the experimental conditions of the mice. Interscapular BAT depots were excised from 3-month and 2-year-aged mice following euthanasia and fixed in 2% glutaraldehyde in 0.1 M cacodylate buffer. A heavy metal protocol was used for processing. Samples were: washed with deionized H_2O (diH_2O) and then immersed in 3% potassium ferrocyanide, followed by 2% osmium tetroxide, at 4°C for 1-h each; immersed in filtered 0.1% thiocarbohydrazide for 20 min following diH_2O wash; washed again in diH_2O and then immersed in 2% osmium tetroxide for 30 min.; incubated overnight in 1% uranyl acetate at 4°C before incubation in 0.6% lead aspartate for 30 min at 60°C. An ethanol-graded series dehydration was then performed before samples being infiltrated with epoxy Taab 812 hard resin. Samples were then immersed in fresh resin and polymerized at 60°C for 36–48 h. Transmission electron microscopy (TEM) was utilized to identify regions of interest for each of the resultant resin blocks. Samples were trimmed and glued to an SEM stub before being placed into a FEI/Thermo Scientific Volumescope 2 SEM. 300–400 serial sections of 0.09 µm thickness were then obtained and collected per sample block. The micrograph blocks were then aligned, manually segmented, and 3D-reconstructed using Thermo Scientific Amira Software (Garza-Lopez et al., 2022; Hinton et al., 2023; Neikirk, Vue, et al., 2023).

2.3 | Mitochondrial and LD ultrastructure calculations and measurements

Label analyses were performed following manual segmentation of LDs and lipid-associated mitochondria in the regions of interest (ROIs). Each segmented structure was then subject to label analysis using Amira (Garza-Lopez et al., 2022). Experiments were performed at least three independent times to obtain the SBF-SEM murine BAT data. 300-400 sequential orthoslices were obtained for each 3D reconstruction. 50–200 serial sections were then chosen at approximately equal z-direction intervals. Serial sections were then stacked, aligned, and visualized using Amira software. All videos and volumetric structure quantifications were generated using Amira software. Measurement algorithms that were not already in the

system were manually entered. All mitochondria associated with LDs were manually segmented (Figure 2). A total of ~800 (3 months) and ~1100 (2 years) mitochondria associated with LDs were collected for quantification from six total mice (n = 3).

2.4 | Western blot analysis

Tissue from adult (3 months) and aged (2 years) mice were collected, as described above, and lysed RIPA lysis buffer (1% NP40, 150 mM NaCl, 25 mM Tris base, 0.5% sodium deoxycholate, 0.1% SDS), 1% phosphatase inhibitor cocktails #2 (Sigma P5726-1ML)/#3 (Sigma P0044-1ML), and one complete protease inhibitor tablet (Sigma 04693159001). Following protein solubilization, quantification was performed using a BCA Assay (VLBL00GD2; Thermo Scientific). Equal protein amounts were then separated on 4%–20% Tris-glycine gels (WXP42012BOX; Invitrogen). Following electrophoresis, proteins were transferred to a nitrocellulose membrane (926-31092; Li-Cor) and incubated overnight at 4°C with primary antibodies: Mic60/mitofilin (ab110329; Abcam) and beta Actin (MA5-15739-HRP). The mitofilin membrane was incubated for 1 h at room temperature with secondary antibodies, diluted 1:10,000: donkey anti-mouse IgG (H+L) (A32789; Invitrogen). Blots were visualized using the Invitrogen iBright imaging system.

2.5 | Structure quantifications and statistic analyses

Statistical analyses and manual measurements of all data were analyzed using a Student's t test, or the nonparametric equivalent where applicable, in GraphPad Prism. Individual data points are depicted by dots and all data are considered biological replicates unless otherwise specified. All outliers were used for statistical analyses but may not be displayed for presentation purposes. Graphs are depicted as means with standard error mean (mean ± standard error of the mean) indicated as black bars. Statistical significance was defined as $p < 0.05$ (*), $p < 0.01$ (**), $p < 0.001$ (***), and $p < 0.0001$ (****).

3 | RESULTS

3.1 | Murine BAT contains smaller LDs across aging with no changes in total cellular lipid volume

Cohort age groups were selected as 3 months, which is considered life phase equivalent to 20 years of age in humans, and 2 years, which is considered approximately 69 years of age in humans (Dutta & Sengupta, 2016). Following intrascapular BAT tissue extraction, SBF-SEM was utilized to examine the 3D dynamics of both LDs and, as it provides a high (with out image block reconstruction at 10 µm for the x- and y-axis and 50 µm for the z-axis) while also allowing for large volumes to be surveyed (Marshall et al., 2023). 3D reconstructions were performed using previously described methods (Neikirk, Vue, et al., 2023); for each age cohort (n = 3) approximately 150–300 LDs were surveyed, for a total of ~500 LDs reconstructed (Figure 1a). 3D reconstruction was performed by the manual contour tracing of 50 images of 50-µm block orthogonal (ortho) slices (Figure 1b) across standard transverse intervals (Figure 1c) to enable the reconstruction of pseudocolored LDs (Figure 1d).

Using this workflow of SBF-SEM-based 3D reconstruction, orthoslices (Figure 2a) were overlaid for 3D reconstruction (Figure 2a) of LDs. Based on these representative orthoslices, detailed 3D reconstruction of LDs were rendered (Figure 2a,a′,a″) in both 3-month (young) (Video S1) and 2-year (aged) (Video S2) samples (Figure 2b,b′,b″).

Notably, in young samples, we noticed that many individual LDs were too large to fit inside the region of interest, despite the relatively large range of SBF-SEM (10 µm by 10 µm) (Marshall et al., 2023). Although this means that the values for young samples are less reliable, it also supports the notion that aging results in decreased LD volume. This was validated by the significant decrease in LD 3D area (Figure 2c), volume (Figure 2d), and perimeter (Figure 2f) in aged samples compared to young samples (Videos S3 and S4). Furthermore, it is unlikely this occurred due to some lipids falling outside of the range of the ROI, as the total cellular volume with lipids showed a marked, although statistically insignificant, decrease (Figure 2e). When comparing the LD quantification from each mouse, there was minor variability between samples within each group but consistent differences between groups (Figure 2c′–f′). Together, this indicates an age-dependent loss in LD total size and average size.

Past studies have demonstrated a way to organize mitochondria in a karyotype-like arrangement on the basis of volume (Crabtree et al., 2024; Vincent et al., 2019; Vue, Garza-Lopez, et al., 2022; Vue et al., 2023). Here, we adapt this method to form a "lipid-otype" organization which allows for the structure and complexity of LDs of various, relatively similar volumes to be compared across age conditions (Figure 3a). This shows a relatively even distribution of lipid sizes with increased roundness in aged samples. To verify these changes in the roundness of LDs across BAT aging, we calculated lipid sphericity as $\frac{\pi^{\frac{1}{3}}(6 \times \text{Volume})^{\frac{2}{3}}}{\text{Surface area}}$. We found that LD sphericity increased with aging in BAT (Figure 3b,b′). Consistent with this, we also found that the complexity, which is inversely related to sphericity, of LD 3D structures decreased with age (Figure 3c,c′). This may indicate that bilayer tension and phospholipid asymmetry are increased, leading to altered LD biogenesis (Fader Kaiser et al., 2022).

Together, these findings show an age-dependent decrease in the size and increased sphericity of LDs, consistent with changes in morphology. To better understand if the broader cellular environment was concomitantly altered with these morphological changes, we decided to look at possible changes in mitochondrial interactions with LDs across aging.

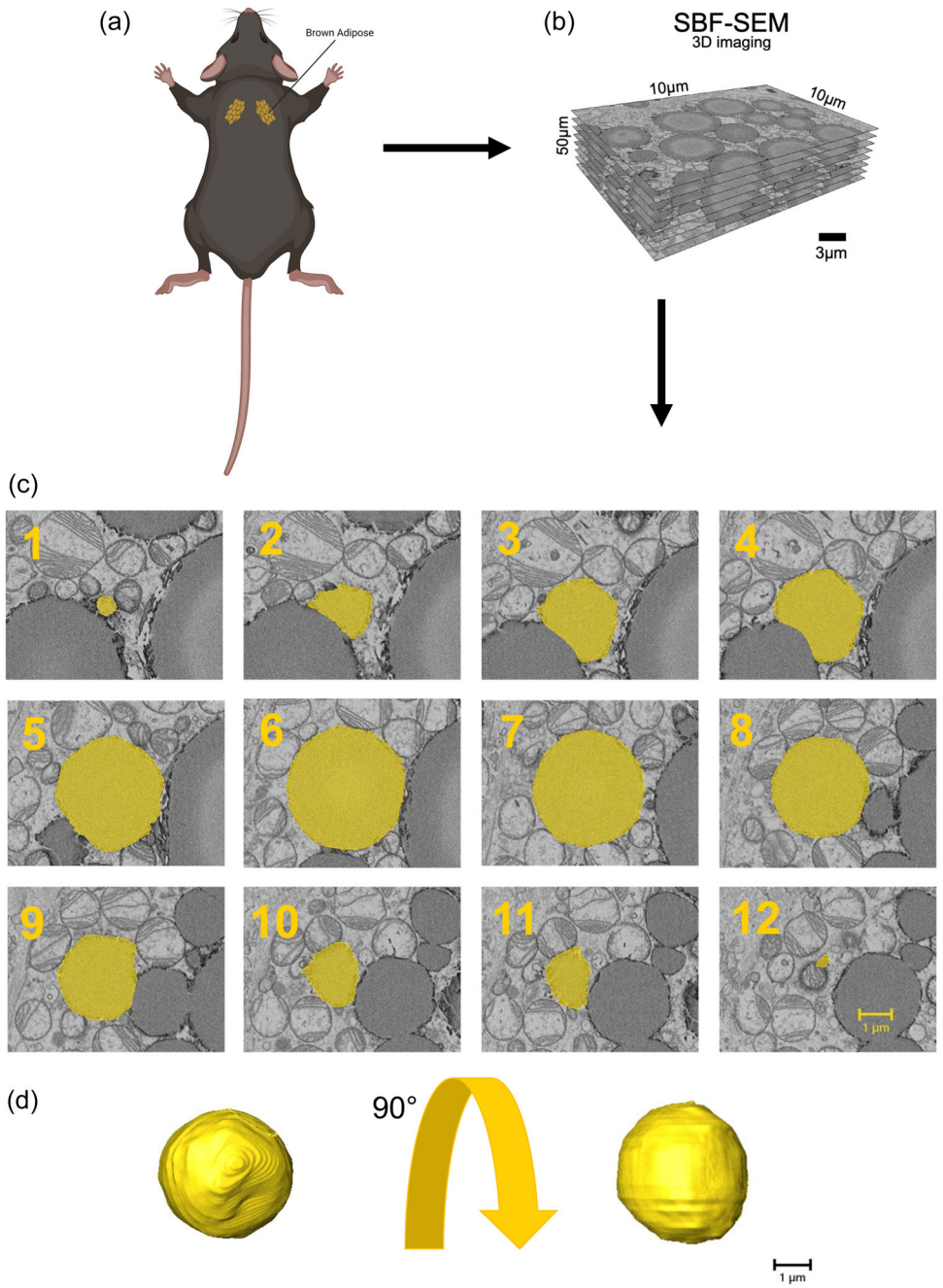

FIGURE 1 Detailed 3D reconstruction workflow for lipid droplets using serial block face-scanning electron microscopy (SBF-SEM). (a) Interscapular brown adipose tissue (BAT) excised from male C57BL/6J mice. (b) Sample block reconstruction at 10 µm for the *x*- and *y*-axis were generated by imaging, aligning, and stacking consecutive ultrathin sections of the sample. (c) SBF-SEM images had lipid droplets manually traced to create 3D representative orthoslices. (d) A detailed 3D reconstruction of lipid droplets was produced based on this workflow, allowing for in-depth analysis of lipid droplet size and complexity. 3D, three-dimensional.

3.2 | BAT 3D reconstruction shows altered mito–lipid interactions across aging

Using the same BAT ROIs that were used for LD quantifications, we sought to quantify the mitochondria–lipid interactions in both age groups (Figure 4a–e). Using a similar workflow, BAT was extracted from male mice (Figure 4a) and subject to SBF-SEM imaging (Figure 4b). LD-associated mitochondria were identified (Figure 4c), and manual contour tracing was done to calculate the contacts between the mitochondria and the LDs (Figure 4d). Notably, we found that mitochondria interacted with up to four different LDs simultaneously, owing, in part, to the large volume of LDs in BAT (Figure 4e). Given the high number of interactions, we randomly selected two mice from each age cohort ($n = 2$) and surveyed

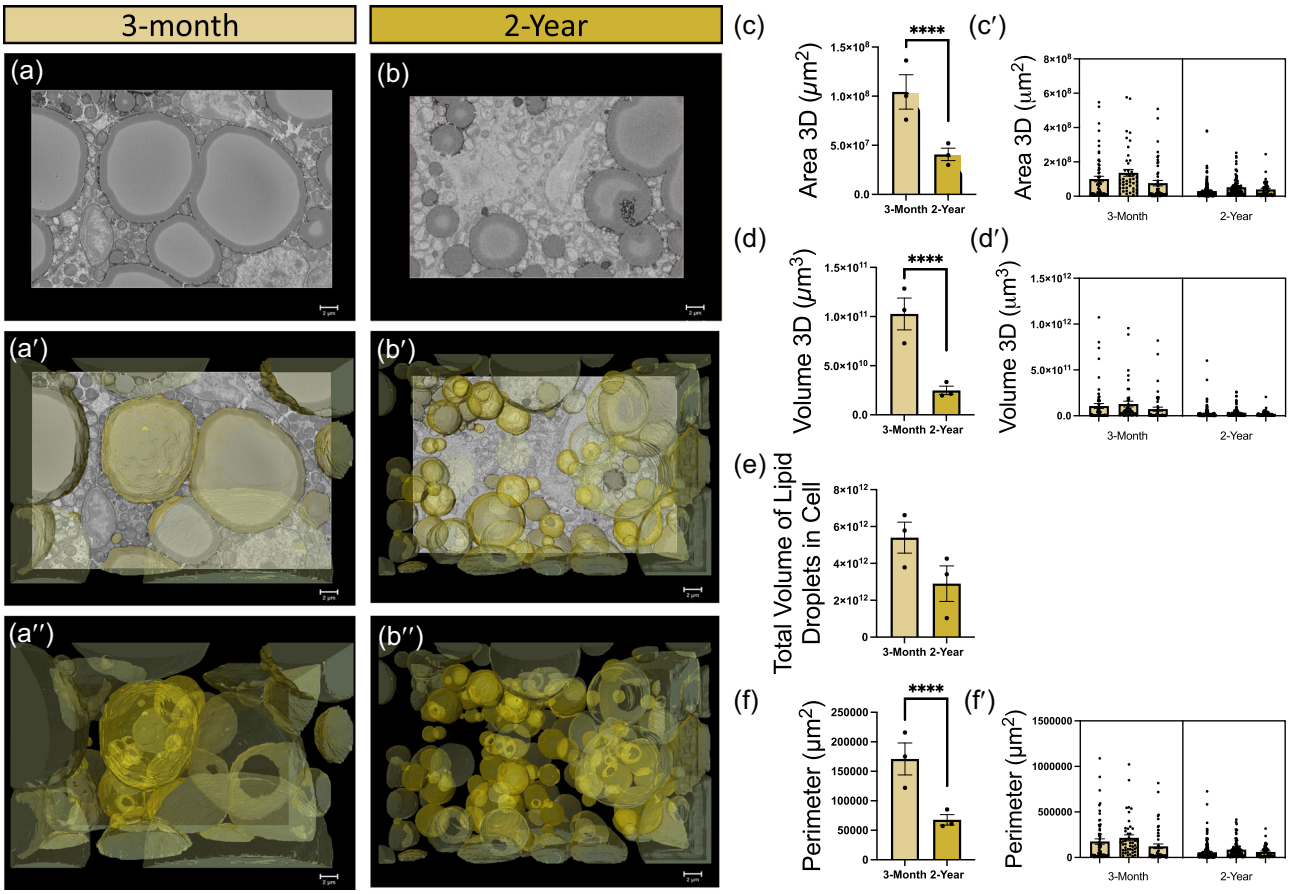

FIGURE 2 Analysis of mitochondrial morphology changes during the aging process. (a) Three-month-old and (b) 2-year-old murine BAT showing: a representative orthoslice; (a′) and (b′) 3D reconstruction of lipid droplet overlaid on the orthoslice; (a″) and (b″) Isolated 3D reconstruction with orthoslice removed, highlighting the individual lipid droplet structures. (c) Quantitative comparison of 3D lipid droplet area, (d) volume per lipid droplet, (e) cumulative lipid droplet volume, and (f) perimeter between 3-month and 2-year samples to assess morphological differences, revealing age-related changes in size of lipid droplets. Unpaired *t* test was used to evaluate changes, with a variable sample number (n = ~75 per mouse), with each individual mouse's average represented by black dots. (c′), (d′), and (f′) Display of raw lipid droplet quantifications. Each bar represents one of the three regions of interest surveyed at respective age points while dots represent individual lipid droplets (n = ~75). Values are displayed for lipid (c′) area, (d′) volume, and (f′) perimeter. In total, 159 lipid droplets across three 3-month male mice and 367 lipid droplets across three 2-year-old male mice were surveyed. The total count of lipid droplets across all mice from each respective age cohort was used for statistical analyses. $p < 0.0001$ indicated by ****. BAT, brown adipose tissue; 3D, three-dimensional.

interactions from these samples for approximately 800 total interactions in 3-month samples and 1100 interactions in 2-year samples.

Using this workflow, we reconstructed LDs (Figure 5a′,b′), mitochondria (Figure 5a″,b″), and the contact points between the two organelles (Figure 5a‴,b‴) (Videos S5 and S6). We found no statistically significant change in the percent of total mitochondria present interacting with LDs in aged samples (Figure 5c). Interestingly, when disaggregating on the basis of the number of contacts formed, we observed that single interactions were rarer in aged samples, while the proportion of mitochondria interacting with 2, 3, or 4 LD was slightly higher in aged samples (Figure 5d,e). Next, we wanted to see if there were any changes in the mitochondrial and LD surfaces interacting in these aged samples (Figure 5f–l).

Aged samples demonstrated a decrease in both the percent of the mitochondrial perimeter and the surface area in contact with LDs (Figure 5f,h; Videos S7 and S8). In contrast, the percentage of LD perimeter in each interaction in contact with mitochondria increased significantly with aging, likely due to the smaller size and increased abundance of LDs in the aged group (Figure 5g). There was a similar age-dependent increase for LD surface area in contact, occupying a higher proportion of total LD volume (Figure 5i). While these quantifications measured only the relative size of single interactions, given many LDs engaged in multiple contacts, we also totaled the surface area of all contacts each LD engaged in and compared it to the overall surface area of the LD (Figure 5j). This mirrors the findings of individual contacts, showing that contacts increased relative to LD surface area, from 10% in young samples to about 15% in aged samples (Figure 5j). Together, this indicates that, with age, a lower percentage of the total surface of mitochondria is dedicated to mitochondria–LD interactions, while the inverse is true for LDs with both individual and cumulative interactions occupying a large proportion of the LD area and perimeter.

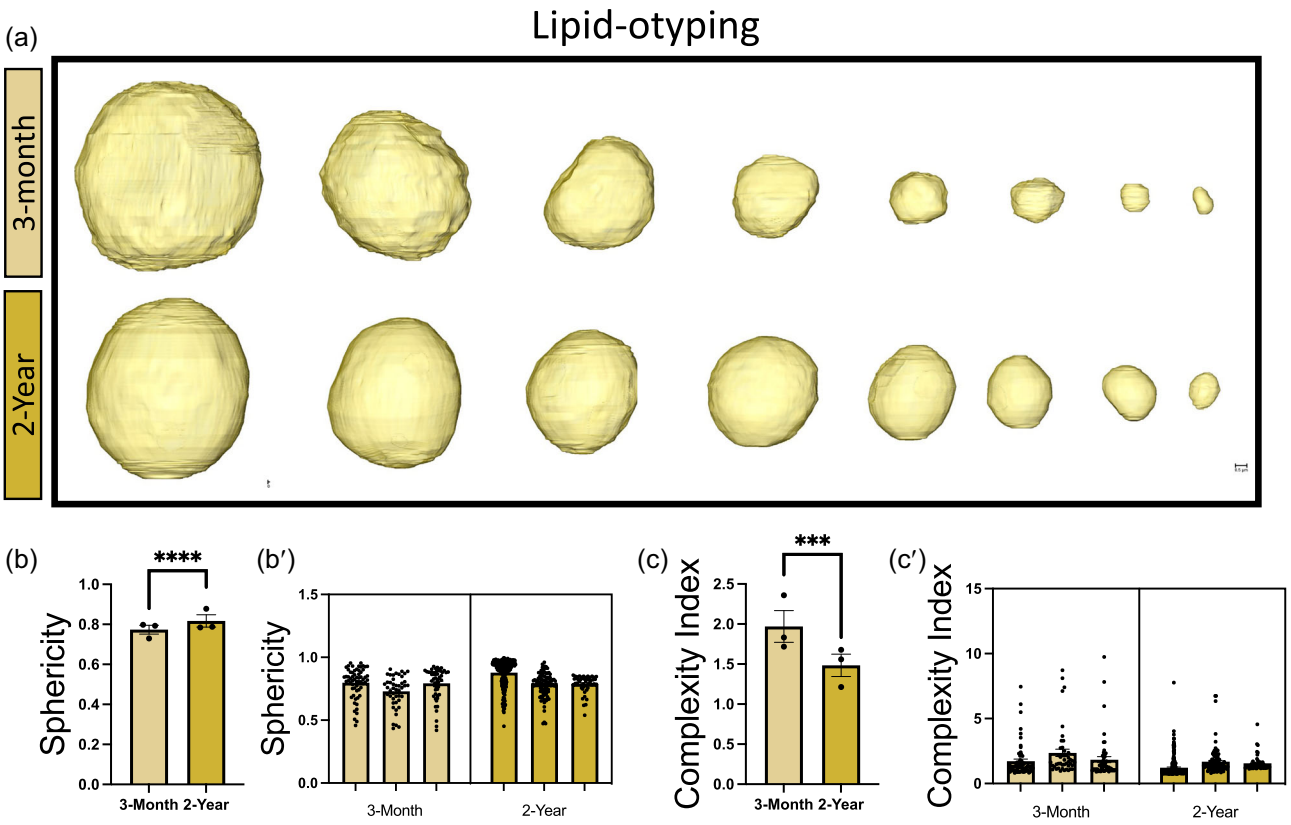

FIGURE 3 Analysis of age-related changes in lipid complexity. (a) Lipid-otyping for lipid droplet morphology in 3-month and 2-year murine BAT samples based on volume, providing insights into the age-related alterations in structural complexity. These changes are seen quantitatively with a comparison of (b) 3D sphericity and (c) complexity index. Unpaired *t* test was used to evaluate changes, with a variable sample number, with each individual mouse's average represented by black dots. (b′) and (c′) display of raw lipid droplet quantifications. Each bar represents one of the three regions of interest surveyed at respective age points while dots represent individual lipid droplets (n = ~75) for (b′) sphericity and (c′) complexity index. In total 159 lipid droplets across three 3-month male mice and 367 lipid droplets across three 2-year-old male mice were surveyed. The total count of lipid droplets across all mice in respective age cohorts was used for statistical analysis. $p < 0.001$ and $p < 0.0001$ are indicated by *** and ****, respectively. BAT, brown adipose tissue; 3D, three-dimensional.

Contact sites can be measured by the tightness of their junctions and their impact on modulating the structure of each organelle. Therefore, we examined age-related changes that occur at the contact sites themselves. This led us to discover a significant decrease in the average volume and surface area of each mitochondria–LD contact across aging (Figure 5k,l). This indicates that the contact sites are decreasing in surface area, with a potential tightening of these contacts resulting in reduced volume. Notably, there was a large sample heterogeneity between the two ROIs surveyed, indicating both intra- and inter-sample variance (Figure 5f′–l′).

3.3 | 3D reconstruction shows mitochondria–LD interactions do not cause alterations in mitochondrial morphology

We questioned if cytosolic mitochondria would differ in morphology, and therefore function, compared to those interacting with LDs (Jenkins et al., 2024). Significant contact was defined as mitochondria with >20% of the mitochondria perimeter interacting with LDs (Benador et al., 2018). It has been reported that subpopulations of mitochondria are functionally distinct from each other (Yu et al., 2015). While we previously considered all mitochondrial volume in aged BAT samples (Crabtree et al., 2024), here, we sought to classify the phenotypes of the mitochondrial subpopulations. Using the same two ROIs, manual contour tracing was used for 3D reconstruction in young (Figure 6a) and aged (Figure 6b) BAT. LD-associated and cytoplasmic mitochondria were distinguished, 3D reconstructed, and overlaid on orthoslices (Figure 6a′,b′) or viewed with the LDs present in the sample (Figure 6a″,b″). These interactions were assessed from multiple viewpoints to validate the analysis (Figure 6c,d). Consistent with our previous results (Peres Valgas da Silva et al., 2022), mitochondrial height and width both increased with age (Figure 6e,f). Yet, there were generally insignificant differences in mitochondrial width and height due to LD interactions, with intergroup heterogeneity more readily attributed to age-related differences. However, we observed that cytoplasmic mitochondrial height was unchanged with age, while mitochondria LD-associated mitochondria were significantly increased, indicating that age-related

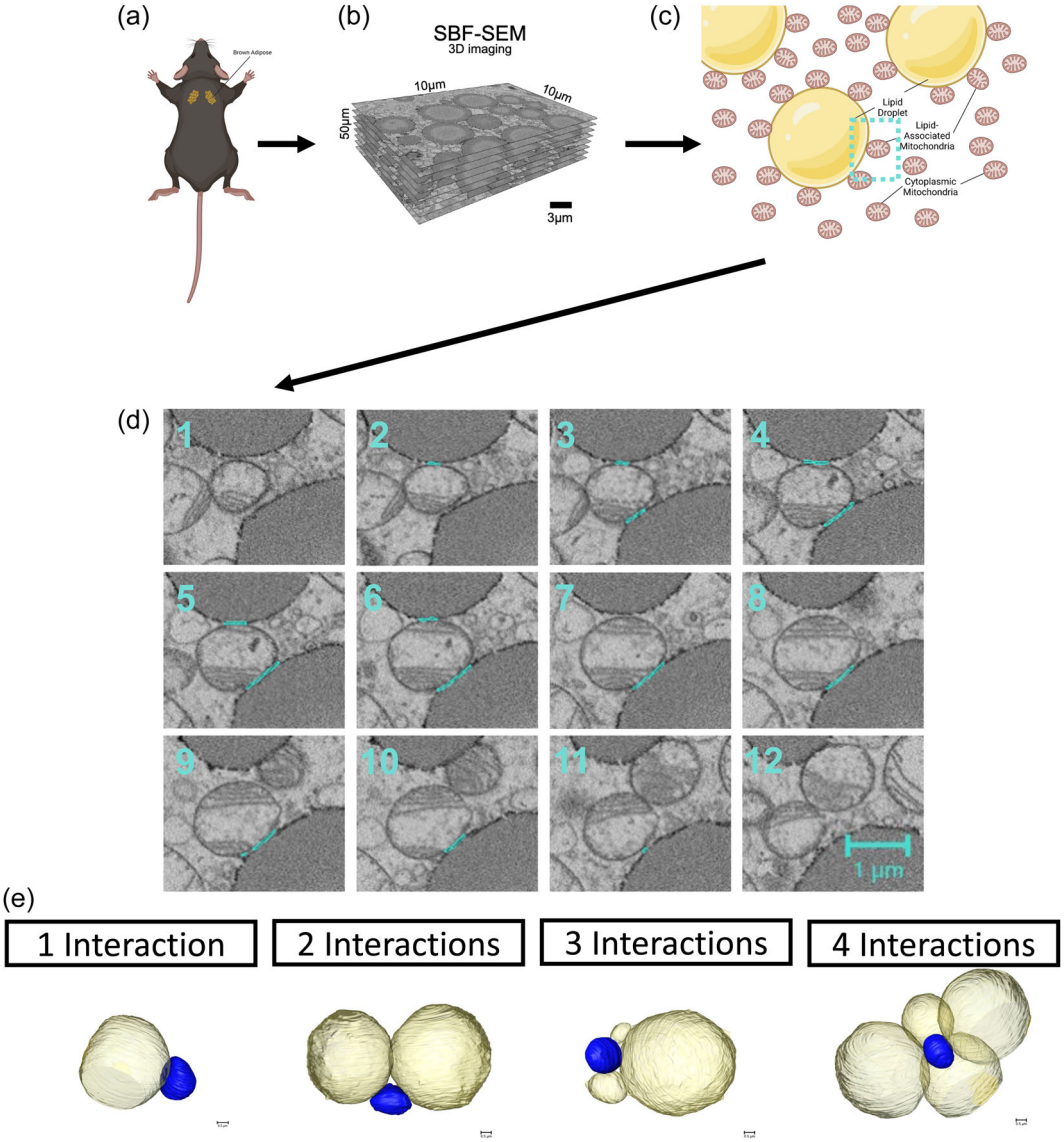

FIGURE 4 Workflow of serial block face-scanning electron microscopy-based 3D reconstruction for mitochondria–lipid interactions. (a) Brown adipose tissue was excised from 3-month and 2-year-aged male C57BL/6J mice. (b) 10 μm by 10 μm orthoslices were overlaid for 3D reconstruction. (c) Lipid-associated mitochondria were identified and (d) manually contour traced, as shown in representative orthoslices from SBF-SEM slices. (e) Diagram of representative images of 1, 2, 3, and 4-lipid droplet interacting mitochondria. 3D, three-dimensional.

changes in mitochondrial size may be more drastic for mitochondrial subpopulations with close proximity to LDs. Together, these results indicate that, while the size of mitochondria–LD interactions changed across aging, the subpopulations of mitochondria may not always dynamically change in response to these alterations in contact sites.

3.4 | Mitochondria–LD interactions may protect cristae from age-related deterioration

To determine how LD associations may affect mitochondrial bioenergetics, we assessed how cristae structure is altered in aging. To assess cristae abundance and structure, we used a 3D metric of cristae scoring (Crabtree et al., 2024; Eisner et al., 2017) assigning a score ranging from 0 to 4 based on the presence and regularity of cristae within the mitochondria. Aging resulted in a significant decrease in cristae quality for both LD-associated and cytoplasmic mitochondria populations (Figure 6h), consistent with our previous published results (Crabtree et al., 2024). While there was no difference in cristae score between LD-associated and cytoplasmic mitochondria populations at 3 months, comparisons among the 2-year-old cohorts show that LD-associated mitochondria populations have a significantly higher cristae score. This suggests that LD interactions may prevent or slow age-related cristae deterioration, thus providing a potential avenue through which LD interactions maintain healthy bioenergetics. Mechanistically, we briefly looked at Mic60 (also known as mitofillin), a member of the mitochondrial inner membrane complex (MICOS), that regulates cristae structure (Anand et al., 2021) and morphology (Fader Kaiser et al., 2022). We

previously reported that MICOS protein levels decrease with aging in cardiac and skeletal muscle tissue (Vue, Garza-Lopez, et al., 2022; Vue et al., 2023). Therefore, we examined the expression of Mic60 in our BAT aging model and found that levels were decreased (Figure 6h), consistent with our previous studies. These observations could indicate possible mechanisms by which mitochondria–LD interactions may protect against age-related loss of cristae integrity, but more research is needed before any inferences can be made.

4 | DISCUSSION

In the present study, 3D quantifications were used to demonstrate that LDs and the mitochondria that interact with them exhibit distinct age-related differences in male murine BAT. We found age-dependent losses in size, as well as changes in the distribution and shape of BAT LDs. These findings are contradictory to other reports of increased cytoplasmic LD size in BAT with

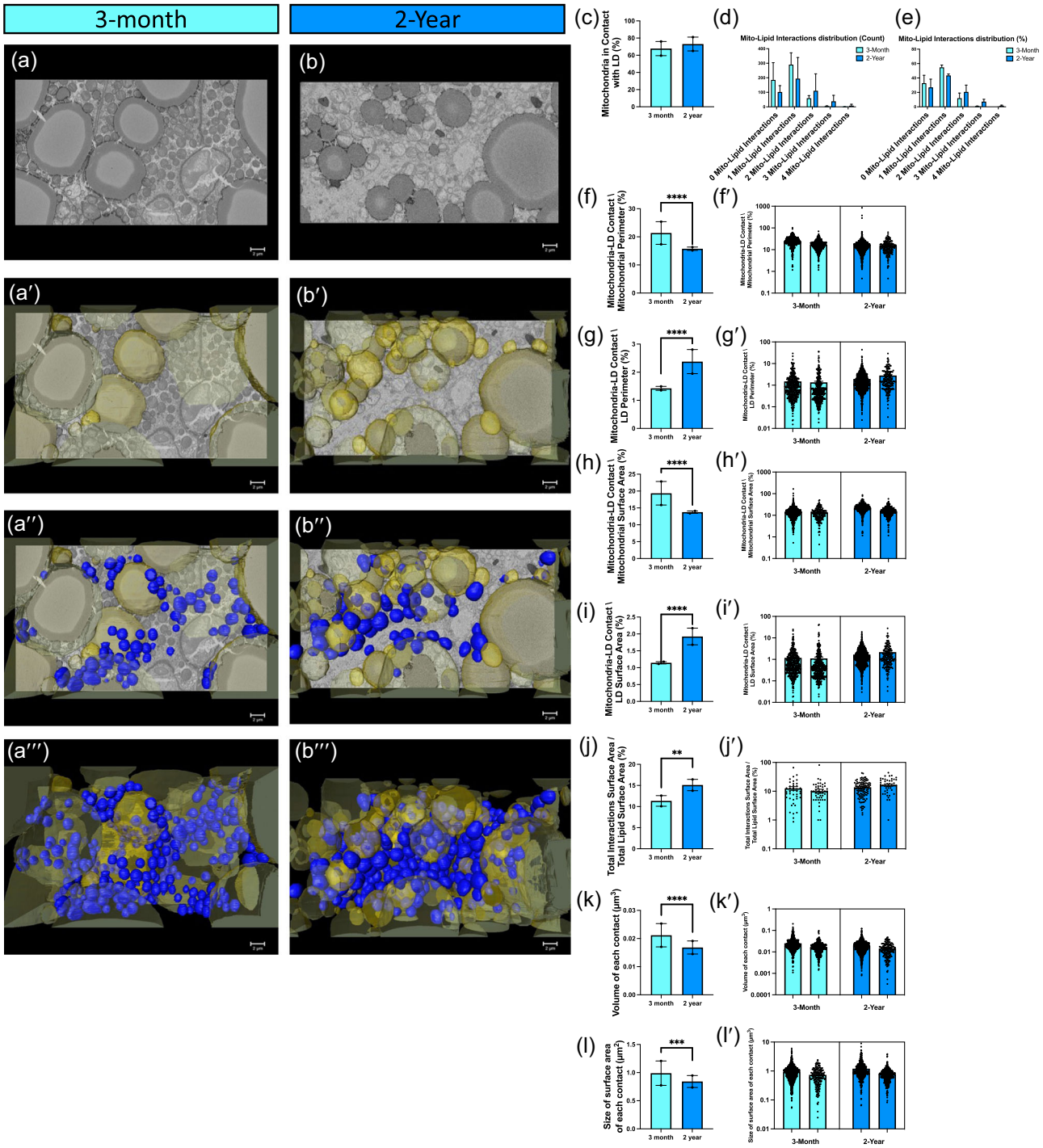

FIGURE 5 (See caption on next page).

aging in both male (Sellayah & Sikder, 2014) and female (Gonçalves et al., 2017) mouse models. However, it should be noted that different subpopulations of brown adipocytes exist, with low-thermogenic activity populations exhibiting larger LDs, whereas high-thermogenic brown adipocytes have smaller LDs (Song, Dai, et al., 2020). Additionally, numerous factors could contribute to the variance observed, including, but not limited to, differences in chow diet composition, microbiome, and housing conditions, among other things. Moreover, previous studies did not quantify LD size using 3D methods, which likely contributed to the reported differences. Notably, our results indicate that there is increased mitochondria–LD interaction surface area relative to total lipid surface area with aging.

Mechanistically, previous lipidomic studies indicate that aging causes dysregulated lipid homeostasis, marked by the inhibition of brown adipogenesis with the concomitant accumulation of specific lipid classes (Gohlke et al., 2019). Furthermore, the activity of BAT across the course of life may dictate lipid synthesis, as aging is associated with decreased mitochondrial uncoupling protein 1 (UCP1) expression, as well as altered endocrine functions which may collectively affect lipolysis and thermogenesis in aging population (Nirengi & Stanford, 2023). It may be that the smaller LDs observed are representative of enhanced lipolytic processes within BAT, leading to increased breakdown of triglyceride stored in LDs (Nirengi & Stanford, 2023). This increased lipolysis could result in the mobilization of fatty acids from LDs and their subsequent utilization for energy production during thermogenesis. Because mitochondrial lipoylation is decreased with age (Tajima et al., 2019), LDs may have a compensatory role, increasing utilization of fatty acid metabolism. Therefore smaller LDs may provide a more readily available pool of fatty acids for oxidation compared to larger LDs, enhancing thermogenic capacity. However, as previously reviewed, the complex nature of lipolysis means that smaller LDs are not always indicative of increased lipolysis (Zadoorian et al., 2023). This is highlighted by reports showing decreased markers of lipolysis and blunted thermogenesis in response to cold exposure in aged murine tissue (Sellayah & Sikder, 2014). Therefore, future mechanistic studies are needed before attempting to define the cause of the smaller LDs observed in our samples.

It is well known that cold-induced activation of murine BAT increases UCP1, a key protein that permits BAT to dissipate heat, in addition to cristae biogenesis (Song, Dai, et al., 2020). These observed alterations in mitochondrial function and ultrastructure have been reported to occur concomitantly with increased formation of mitochondria–LD associations (Yu et al., 2015). Previous reports also indicate that UCP1 activity reduces across aging in BAT (Corrales et al., 2019; Mancini et al., 2021), suggesting there would be reduced and LD–mitochondria contact formation. However, these are not the results that we observed in our samples (Figures 5 and 6). It is possible that distinct UCP1-dependent and -independent pathways exist for LD–mitochondria formation. Notably, different subpopulations of adipocytes have been reported, with low thermogenic activity populations exhibiting larger LDs, while cold treatment causes the dynamic interconversion to high-thermogenic activity adipocytes which have smaller LDs (Song, Dai, et al., 2020). A key hallmark of metabolic syndrome, or greater risk for type II diabetes and cardiovascular disease, caused by a high-fat diet has been the accumulation of LDs (Zhou et al., 2020). Together, these data suggest that UCP1-independent reductions in LD size and the inverse increase in mitochondria–LD contact sites may serve as a compensatory mechanism to avoid metabolic syndrome and increase BAT efficiency. However, this is potentially only one of many possiblilies, warranting the need for further investigation.

Interestingly, we also noticed mitochondria–mitochondria interactions, marked by a shortening of conact site distances, occurring

FIGURE 5 Changes in mitochondria–lipid droplet morphology and frequency across aging. (a) and (b) Murine BAT representative orthoslice, (a′) and (b′) 3D reconstruction of lipid droplet (yellow) overlaid on orthoslice, (a″) and (b″) 3D reconstruction of lipid droplet (yellow) and mitochondria (blue) overlaid on orthoslice, and (a‴) and (b‴) 3D reconstruction mitochondria and lipid droplets in (a)–(a‴) 3-month and (b)–(b‴) 2-year samples. (c)–(i) Quantification of the lipid droplet–mitochondria contact sites. (c) Comparisons of proportion of lipid-associated mitochondria to cytoplasmic mitochondria. (d) Mitochondrial distribution on the basis of number of lipid interactions formed by count and (e) relative percent. (f) percent contact site perimeter coverage relative to total mitochondrial perimeter, (g) percent contact site perimeter coverage relative to total lipid perimeter, (h) percent contact site surface area coverage relative to total mitochondrial surface area, (i) percent contact site surface area coverage relative to total lipid droplet surface area, (j) percent total contact site surface area coverage relative to total lipid droplet surface area. The average (k) volume of each contact, and (l) surface area of each contact were further elucidated. (f′–l′) Display of heterogeneity in mitochondria–lipid droplet interactions. Each bar represents one of the two regions of interest surveyed at respective age points while dots represent individual contact sites (n = ~400). Values are displayed for (f′) percent contact site perimeter coverage relative to total mitochondrial perimeter, (g′) percent contact site perimeter coverage relative to total lipid perimeter, (h′) percent contact site surface area coverage relative to total mitochondrial surface area, (i′) percent contact site surface area coverage relative to total lipid droplet surface area, (j′) percent total contact site surface area coverage relative to total lipid droplet surface area, (k′) volume of each contact, and (l′) surface area of contact. Unpaired t test was used to evaluate changes, with a variable sample number (n = ~400), with each individual mouse's average represented by black dots. For "total lipid area in interactions," a total of 94 lipid droplet–mitochondria interactions were surveyed across two 3-month male mice, and 163 lipid droplet–mitochondria interactions were surveyed across two 2-year male mice. For all other quantifications of lipid droplet interactions, a total of 839 lipid droplet–mitochondria interactions were surveyed across two 3-month male mice, and 1143 lipid droplet–mitochondria interactions were surveyed across two 2-year male mice. The total count of lipid droplet–mitochondria interactions across all mice in respective age cohorts was used for statistical analyses. $p < 0.05$, $p < 0.01$, $p < 0.001$, and $p < 0.0001$ are indicated by *, **, ***, and ****, respectively. BAT, brown adipose tissue; 3D, three-dimensional.

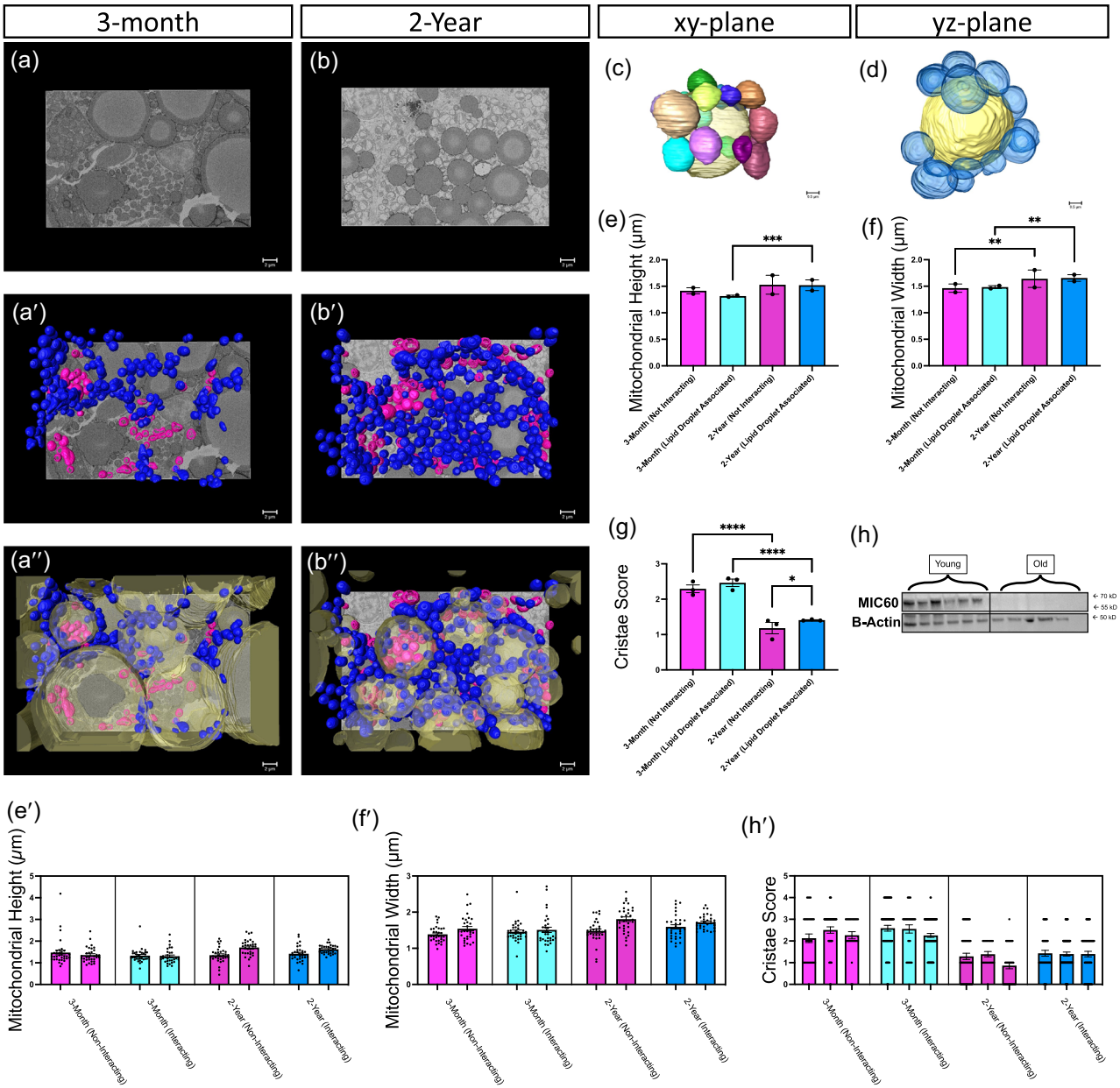

FIGURE 6 Lipid-associated mitochondria show distinct subpopulation changes in mitochondrial ultrastructure. (a) Three-month murine BAT mitochondria viewed from orthoslice, allowing for fine details to be visualized; (a′) reconstruction of cytoplasmic (pink) and lipid-associated (blue) mitochondria; (a″) 3D reconstruction of isolated mitochondria and lipid-associated mitochondria with lipid droplets present. (b) 2-year murine BAT mitochondria viewed from orthoslice, allowing for fine details to be visualized; (b′) reconstruction of cytoplasmic (pink) and lipid-associated (blue) mitochondria; (b″) 3D reconstruction of isolated mitochondria (pink) and lipid-associated mitochondria with lipid droplets present. (c) Mitochondria associations with lipid droplets viewed from the *xy* plane and (d) *yz* plane. (e) Comparisons of mitochondrial 3D height and (f) width across aging and on the basis of age and if interacting with lipid droplets. (g) Cristae score, a metric scored from 0 to 4, of mitochondria compared across aging and interaction status of mitochondria. (h) Western blot analysis of Mic60 in murine BAT comparing 3-month and 2-year tissue samples. (e′)–(h′) Variation within mitochondrial and cristae quantifications. Each bar represents one of the two or three regions of interest surveyed at respective age points while dots represent individual mitochondria (n = ~33 for mitochondria; n = ~50 for cristae, with high variability). Values are displayed for (e′) mitochondrial height, (f′) mitochondrial width, and (g′) cristae score. Kruskal–Wallis one-way analysis of variance with post hoc pairwise comparison test comparing each mean of groups, was used to evaluate changes, with a variable sample number (n = ~33 for mitochondria; n = ~50 for cristae) with each individual mouse's average represented by black dots. For mitochondrial height and width, in total, 65 mitochondria not interacting with lipid droplets in two 3-month male mice, 65 mitochondria interacting with lipid droplets in two 3-month male mice, 65 mitochondria not interacting with lipid droplets in two 2-year male mice, and 65 mitochondria interacting with lipid droplets in two 2-year male mice were surveyed. For mitochondrial cristae score, in total, 102 mitochondria not interacting with lipid droplets in three 3-month male mice, 173 mitochondria interacting with lipid droplets in three 3-month male mice, 115 mitochondria not interacting with lipid droplets in three 2-year male mice, and 185 mitochondria interacting with lipid droplets in three 2-year male mice were surveyed. The total count of mitochondria across all mice in respective age cohorts were used for statistical analysis. $p < 0.05$, $p < 0.01$, $p < 0.001$, and $p < 0.0001$ are indicated by *, **, ***, and ****, respectively. BAT, brown adipose tissue; 3D, three-dimensional.

between mitochondria interacting with LDs and those not interacting (Figure 5). It is possible this is a tri-organelle contact site, as has previously been reported through ER, mitochondria, and peroxisomes (Ilacqua et al., 2021). However, the functional relevance of mitochondria–mitochondria contact sites has not been well established. Equally possible, these decreased mitochondrial separation distances may be indicative of post- or premitochondrial dynamic events (Brandt et al., 2016). Similarly, we also many mitochondria were interacting with more than one LD. It is possible that bioenergetics differ based on the quantity of LDs interacting with each mitochondrion. Notably, we did not consider how mitochondrial quantification changed with the number of interactions. Thus, future studies may explicate if there are significant differences when considering mitochondrial quantification on the basis of LD interaction count or tri-organelle contact.

As LD-associated mitochondria change in architecture compared to cytoplasmic mitochondria, it is possible that they support the growth of LDs for future triglyceride lipolysis through alterations in bioenergetics. Changes in mitochondrial–LD interactions may affect the efficiency of energy production and thermogenesis, leading to impaired lipid utilization and compromised mitochondrial function in aged BAT (Benador et al., 2018; Freyre et al., 2019; Yu et al., 2015). Furthermore, in aged samples, cristae remain more stable in structure if they have LD interactions (Figure 6h), suggesting that these interactions may be protective. It should be noted that there are two types of mitochondria-LD interactions that have been reported: (1) anchored or "stable" LD–mitochondrial contact sites (Chen et al., 2022; Yang et al., 2022; Yu et al., 2015) and (2) dynamic interactions of the peridroplet mitochondria that are believed to have distinct functional roles (Benador et al., 2018; Acín-Perez et al., 2021). Although here, we could not biochemically differentiate between these subpopulations, our results could be the result of variable subpopulation frequency changes that might occur with aging. This could account for differences observed by others that bound LD-mitochondrial interactions resulted in LD expansion (Benador et al., 2018). However, further studies are warranted to determine if this is a possibility.

There are several important limitations of our study that should be noted. First, studies show that there are distinct populations of brown adipocytes with either high or low thermogenic activity. Aside from different expression levels of *Ucp1*, these adipocytes also differ in LD size and mitochondrial content (Song, Dai, et al., 2020). Our study did not account for this heterogeneity with in the BAT samples, which may contribute to some of the variation observed in organelle morphology. Future studies may consider 3D tissue profiling to see if contact site structure varies across populations of adipocytes or *Ucp1* expression (Song, Dai, et al., 2020). Additionally, while LDs and mitochondria form dynamic contact sites, they can also form tight-bound interactions (Acín-Perez et al., 2021; Benador et al., 2018; Cui et al., 2019; Cui & Liu, 2020). These interactions are in contrast to mitochondria–endoplasmic reticulum contact sites, which have clearly defined thickness (Giacomello & Pellegrini, 2016). Currently, the distance between dynamic and tight/stable LD–mitochondria interactions remains poorly studied, limiting the ability for differentiation and comparison using 3D reconstruction.

It is also important to note that while murine model allows for studying BAT across aging, it can also differ from human BAT. Interscapular BAT, as studied here, is not often present exist in humans beyond early childhood; the thermogenic role of BAT is more essential to small rodents than to humans (Samuelson & Vidal-Puig, 2020). This makes the roles of human BAT less clear, especially in the context of the age-dependent loss of BAT observed in humans (Samuelson & Vidal-Puig, 2020). Additionally, only male mice were used in this study. This is important to note as sexual dimorphism has relevance in physiological function, given that BAT from women can display altered expression of certain proteins such as UCP1 (Lee & Fried, 2017; Nadal-Casellas et al., 2013). Previous studies also show that there is a correlation between insulin resistance and adipocyte size in male mice but no in female mice (Gonçalves et al., 2017). Additionally, those findings suggest that tri-iodothyronine may maintain UCP1 synthesis in female mice, allowing them to maintain thermogenic capacity across the aging process (Gonçalves et al., 2017). Furthermore, sex-dependent differences can manifest in distinct processes, such as puberty, where BAT is more abundant and active in males (Gómez-García et al., 2022). Although there are commonalities in BAT across sexes, possible sex-dependent differences should be considered in the interpretation of these results.

Overall, this study defines the age-related changes in LD 3D morphology and mitochondria–L Dinteractions, which could collectively contribute to the decline in thermogenic capacity and mitochondrial function in aged BAT. Understanding these changes may provide valuable insights into age-associated metabolic disorders and inform potential therapeutic strategies targeting these dysfunctions. Our studies demonstrate the importance of considering organelle contact sites, rather than focusing solely on mitochondrial morphology when examining structural changes occurring in response to aging.

AUTHOR CONTRIBUTIONS

Amber Crabtree performed the experimental procedures, data analysis, interpretation of results, and writing of the manuscript. Kit Neikirk and Julia A. Pinette contributed equally to this work. They performed the experimental procedures, data analysis, interpretation of results, and writing of the manuscript. Han Le, Bryanna Shao, Aaron Whiteside, Zer Vue, Larry Vang, Trinity Celeste Owens, Ashton Oliver, Faben Zeleke, Heather K. Beasley, Jessica Bedenbaugh, Edgar Garza Lopez, Estevão Scudese, Alice Koh, Suzanne Navarro, Jacob Lam, Kinuthia Kabugi, Ben Kirk, and Margaret Mungai were involved in data collection, analysis, and interpretation. Steven M. Damo, Jennifer A. Gaddy, Clintoria Williams, Jianqiang Shao, Elma Zaganjor, Melanie R. McReynolds, Mariya Sweetwyne, Ho-Jin Koh, Sandra A. Murray, Anthonya Cooper, Mert Demirci, Taseer Ahmad, Taylor Rodman, Han Le, and Annet Kirabo provided critical feedback, contributed to the writing and revision of the manuscript, and assisted in various aspects of the research. Andrea G. Marshal and

Antentor Hinton Jr. conceptualized the study, provided overall guidance, supervised the research, and revised the manuscript.

ACKNOWLEDGMENTS

This study was supported by the UNCF/Bristol-Myers Squibb E.E. Just Faculty Fund, BWF Career Awards at the Scientific Interface Award, BWF Ad-hoc Award, NIH Small Research Pilot Subaward to 5R25HL106365-12 from the National Institutes of Health PRIDE Program, DK020593, Vanderbilt Diabetes and Research Training Center for DRTC Alzheimer's Disease Pilot & Feasibility Program. T-32, number DK007563 entitled Multidisciplinary Training in Molecular Endocrinology to A. C. NSF NRT grant 19-22697 and NSF BPE grant 22-17621 (K. Stassun, PI) to A. C.; T-32, number DK007563 entitled Multidisciplinary Training in Molecular Endocrinology to Z. V. CZI Science Diversity Leadership grant number 2022-253529 from the Chan Zuckerberg Initiative DAF, an advised fund of Silicon Valley Community Foundation (to A. H. J.). NSF EES2112556, NSF EES1817282, NSF MCB1955975, and CZI Science Diversity Leadership grant number 2022-253614 from the Chan Zuckerberg Initiative DAF, an advised fund of Silicon Valley Community Foundation (to S. D.). This work was further supported by NIH grants K01HL130497 (A. K.), R01HL147818 (A. K.), R03HL155041 (A. K.), and R01HL144941 (A. K.) NSF grant MCB #2011577I to S. A. M. NIH K01AG062757 to M.T.S. I01 BX005352 from the Department of Veterans Affairs Office of Research to J. A. G.

CONFLICT OF INTEREST STATEMENT

The authors declare no conflict of interest.

ORCID

Annet Kirabo http://orcid.org/0000-0001-8580-9359
Antentor Hinton http://orcid.org/0000-0002-7730-952X

REFERENCES

Acín-Perez, R., Petcherski, A., Veliova, M., Benador, I. Y., Assali, E. A., Colleluori, G., Cinti, S., Brownstein, A. J., Baghdasarian, S., Livhits, M. J., Yeh, M. W., Krishnan, K. C., Vergnes, L., Winn, N. C., Padilla, J., Liesa, M., Sacks, H. S., & Shirihai, O. S. (2021). Recruitment and remodeling of peridroplet mitochondria in human adipose tissue. *Redox Biology*, *46*, 102087. https://doi.org/10.1016/j.redox.2021.102087

Afzal, N., Lederer, W. J., Jafri, M. S., & Mannella, C. A. (2021). Effect of crista morphology on mitochondrial ATP output: A computational study. *Current Research in Physiology*, *4*, 163–176.

Anand, R., Reichert, A. S., & Kondadi, A. K. (2021). Emerging roles of the MICOS complex in cristae dynamics and biogenesis. *Biology (Basel)*, *10*, 600. https://doi.org/10.3390/biology10070600

Benador, I. Y., Veliova, M., Mahdaviani, K., Petcherski, A., Wikstrom, J. D., Assali, E. A., Acín-Pérez, R., Shum, M., Oliveira, M. F., Cinti, S., Sztalryd, C., Barshop, W. D., Wohlschlegel, J. A., Corkey, B. E., Liesa, M., & Shirihai, O. S. (2018). Mitochondria bound to lipid droplets have unique bioenergetics, composition, and dynamics that support lipid droplet expansion. *Cell Metabolism*, *27*, 869–885.e6. https://doi.org/10.1016/j.cmet.2018.03.003

Boutant, M., Kulkarni, S. S., Joffraud, M., Ratajczak, J., Valera-Alberni, M., Combe, R., Zorzano, A., & Cantó, C. (2017). Mfn2 is critical for brown adipose tissue thermogenic function. *The EMBO Journal*, *36*, 1543–1558.

Brandt, T., Cavellini, L., Kühlbrandt, W., & Cohen, M. M. (2016). A mitofusin-dependent docking ring complex triggers mitochondrial fusion in vitro. *eLife*, *5*, e14618. https://doi.org/10.7554/eLife.14618

Brandt, T., Mourier, A., Tain, L. S., Partridge, L., Larsson, N.-G., & Kühlbrandt, W. (2017). Changes of mitochondrial ultrastructure and function during ageing in mice and Drosophila. *eLife*, *6*, e24662. https://doi.org/10.7554/eLife.24662

Chen, L., Jin, Y., Wu, J., & Ren, Z. (2022). Lipid droplets: A cellular organelle vital for thermogenesis. *International Journal of Biological Sciences*, *18*, 6176–6188. https://doi.org/10.7150/ijbs.77051

Cohen, A. W., Razani, B., Wang, X. B., Combs, T. P., Williams, T. M., Scherer, P. E., & Lisanti, M. P. (2003). Caveolin-1-deficient mice show insulin resistance and defective insulin receptor protein expression in adipose tissue. *American Journal of Physiology-Cell Physiology*, *285*, C222–C235. https://doi.org/10.1152/ajpcell.00006.2003

Corrales, P., Vivas, Y., Izquierdo-Lahuerta, A., Horrillo, D., Seoane-Collazo, P., Velasco, I., Torres, L., Lopez, Y., Martínez, C., López, M., Ros, M., Obregon, M. J., & Medina-Gomez, G. (2019). Long-term caloric restriction ameliorates deleterious effects of aging on white and brown adipose tissue plasticity. *Aging Cell*, *18*, e12948. https://doi.org/10.1111/acel.12948

Courson, J. A., Landry, P. T., Do, T., Spehlmann, E., Lafontant, P. J., Patel, N., Rumbaut, R. E., & Burns, A. R. (2021). Serial block-face scanning electron microscopy (SBF-SEM) of biological tissue samples. *Journal of Visualized Experiments*, *169*, e62045. https://doi.org/10.3791/62045

Crabtree, A., Neikirk, K., Marshall, A. G., Vang, L., Whiteside, A. J., Williams, Q., Altamura, C. T., Owens, T. C., Stephens, D., Shao, B., Koh, A., Killion, M., Lopez, E. G., Lam, J., Rodriguez, B., Mungai, M., Stanley, J., Dean, E. D., Koh, H. J., … Hinton, A. Jr. (2024). Defining mitochondrial cristae morphology changes induced by aging in brown adipose tissue. *Advanced Biology (Weinh)*, *8*(1), e2300186. https://doi.org/10.1002/adbi.202300186

Cui, L., & Liu, P. (2020). Two types of contact between lipid droplets and mitochondria. *Frontiers in Cell and Developmental Biology*, *8*, 8. https://www.frontiersin.org/articles/10.3389/fcell.2020.618322

Cui, L., Mirza, A. H., Zhang, S., Liang, B., & Liu, P. (2019). Lipid droplets and mitochondria are anchored during brown adipocyte differentiation. *Protein & Cell*, *10*, 921–926. https://doi.org/10.1007/s13238-019-00661-1

de-Lima-Júnior, J. C., Souza, G. F., Moura-Assis, A., Gaspar, R. S., Gaspar, J. M., Rocha, A. L., Ferrucci, D. L., Lima, T. I., Victório, S. C., Bonfante, I. L. P., Cavaglieri, C. R., Pareja, J. C., Brunetto, S. Q., Ramos, C. D., Geloneze, B., Mori, M. A., Silveira, L. R., Segundo, G. R. S., Ropelle, E. R., & Velloso, L. A. (2019). Abnormal brown adipose tissue mitochondrial structure and function in IL10 deficiency. *EBioMedicine*, *39*, 436–447. https://doi.org/10.1016/j.ebiom.2018.11.041

Demine, S., Renard, P., & Arnould, T. (2019). Mitochondrial uncoupling: A key controller of biological processes in physiology and diseases. *Cells*, *8*, 795. https://doi.org/10.3390/cells8080795

Dutta, S., & Sengupta, P. (2016). Men and mice: Relating their ages. *Life Sciences*, *152*, 244–248. https://doi.org/10.1016/j.lfs.2015.10.025

Eisner, V., Cupo, R. R., Gao, E., Csordás, G., Slovinsky, W. S., Paillard, M., Cheng, L., Ibetti, J., Chen, S. R. W., Chuprun, J. K., Hoek, J. B., Koch, W. J., & Hajnóczky, G. (2017). Mitochondrial fusion dynamics is robust in the heart and depends on calcium oscillations and contractile activity. *Proceedings of the National Academy of Sciences of the United States of America*, *114*, E859–E868. https://doi.org/10.1073/pnas.1617288114

Eynaudi, A., Díaz-Castro, F., Bórquez, J. C., Bravo-Sagua, R., Parra, V., & Troncoso, R. (2021). Differential effects of oleic and palmitic acids on lipid droplet-mitochondria interaction in the hepatic cell line HepG2. *Frontiers in Nutrition*, *8*, 775382. https://www.frontiersin.org/articles/10.3389/fnut.2021.775382

Fader Kaiser, C. M., Romano, P. S., Vanrell, M. C., Pocognoni, C. A., Jacob, J., Caruso, B., & Delgui, L. R. (2022). Biogenesis and breakdown of lipid droplets in pathological conditions. *Frontiers in Cell and Developmental Biology*, *9*, 826248. https://doi.org/10.3389/fcell.2021.826248

Freyre, C. A. C., Rauher, P. C., Ejsing, C. S., & Klemm, R. W. (2019). MIGA2 links mitochondria, the ER, and lipid droplets and promotes de novo lipogenesis in adipocytes. *Molecular Cell*, *76*, 811–825.e14. https://doi.org/10.1016/j.molcel.2019.09.011

Gao, A. W., & Houtkooper, R. H. (2014). Mitochondrial fission: Firing up mitochondria in brown adipose tissue. *The EMBO Journal*, *33*, 401–402. https://doi.org/10.1002/embj.201487798

Garza-Lopez, E., Vue, Z., Katti, P., Neikirk, K., Biete, M., Lam, J., Beasley, H. K., Marshall, A. G., Rodman, T. A., Christensen, T. A., Salisbury, J. L., Vang, L., Mungai, M., AshShareef, S., Murray, S. A., Shao, J., Streeter, J., Glancy, B., Pereira, R. O., … Hinton, Jr., A. (2021). Protocols for generating surfaces and measuring 3D organelle morphology using amira. *Cells*, *11*, 65. https://doi.org/10.3390/cells11010065

Giacomello, M., & Pellegrini, L. (2016). The coming of age of the mitochondria–ER contact: A matter of thickness. *Cell Death and Differentiation*, *23*, 1417–1427.

Glancy, B., Kim, Y., Katti, P., & Willingham, T. B. (2020). The functional impact of mitochondrial structure across subcellular scales. *Frontiers in Physiology*, *11*, 541040. https://www.frontiersin.org/articles/10.3389/fphys.2020.541040

Gohlke, S., Zagoriy, V., Cuadros Inostroza, A., Méret, M., Mancini, C., Japtok, L., Schumacher, F., Kuhlow, D., Graja, A., Stephanowitz, H., Jähnert, M., Krause, E., Wernitz, A., Petzke, K. J., Schürmann, A., Kleuser, B., & Schulz, T. J. (2019). Identification of functional lipid metabolism biomarkers of brown adipose tissue aging. *Molecular Metabolism*, *24*, 1–17. https://doi.org/10.1016/j.molmet.2019.03.011

Gómez-García, I., Trepiana, J., Fernández-Quintela, A., Giralt, M., & Portillo, M. P. (2022). Sexual dimorphism in brown adipose tissue activation and white adipose tissue browning. *International Journal of Molecular Sciences*, *23*, 8250. https://doi.org/10.3390/ijms23158250

Gonçalves, L. F., Machado, T. Q., Castro-Pinheiro, C., de Souza, N. G., Oliveira, K. J., & Fernandes-Santos, C. (2017). Ageing is associated with brown adipose tissue remodelling and loss of white fat browning in female C57BL/6 mice. *International Journal of Experimental Pathology*, *98*, 100–108. https://doi.org/10.1111/iep.12228

Hinton, A., Katti, P., Christensen, T. A., Mungai, M., Shao, J., Zhang, L., Trushin, S., Alghanem, A., Jaspersen, A., & Geroux, R. E., et al (2023). A comprehensive approach to sample preparation for electron microscopy and the assessment of mitochondrial morphology in tissue and cultured cells. *Advanced Biology (Weinh)*, *7*, e2200202. https://doi.org/10.1002/adbi.202200202

Ilacqua, N., Anastasia, I., Raimondi, A., Lemieux, P., de Aguiar Vallim, T. Q., Toth, K., Koonin, E. V., & Pellegrini, L. (2021). A three-organelle complex made by wrappER contacts with peroxisomes and mitochondria responds to liver lipid flux changes. *Journal of Cell Science*, *135*, jcs259091. https://doi.org/10.1242/jcs.259091

Jenkins, B. C., Neikirk, K., Katti, P., Claypool, S. M., Kirabo, A., McReynolds, M. R., & Hinton, A. (2024). Mitochondria in disease: Changes in shapes and dynamics. *Trends in Biochemical Sciences*, *49*, 346–360. https://doi.org/10.1016/j.tibs.2024.01.011

Johnson, A. A., & Stolzing, A. (2019). The role of lipid metabolism in aging, lifespan regulation, and age-related disease. *Aging Cell*, *18*, e13048. https://doi.org/10.1111/acel.13048

Lam, J., Katti, P., Biete, M., Mungai, M., AshShareef, S., Neikirk, K., Garza Lopez, E., Vue, Z., Christensen, T. A., Beasley, H. K., Rodman, T. A., Murray, S. A., Salisbury, J. L., Glancy, B., Shao, J., Pereira, R. O., Abel, E. D., & Hinton, A. (2021). A universal approach to analyzing transmission electron microscopy with ImageJ. *Cells*, *10*, 2177. https://doi.org/10.3390/cells10092177

Lee, J. H., Park, A., Oh, K.-J., Lee, S. C., Kim, W. K., & Bae, K.-H. (2019). The role of adipose tissue mitochondria: Regulation of mitochondrial function for the treatment of metabolic diseases. *International Journal of Molecular Sciences*, *20*, 4924. https://doi.org/10.3390/ijms20194924

Lee, M.-J., & Fried, S. K. (2017). Sex-dependent depot differences in adipose tissue development and function; role of sex steroids. *Journal of Obesity & Metabolic Syndrome*, *26*, 172–180. https://doi.org/10.7570/jomes.2017.26.3.172

Lippens, S., Kremer, A., Borghgraef, P., & Guérin, C. J. (2019). Serial block face-scanning electron microscopy for volume electron microscopy. *Methods in Cell Biology*, *152*, 69–85.

Mancini, C., Gohlke, S., Garcia-Carrizo, F., Zagoriy, V., Stephanowitz, H., & Schulz, T. J. (2021). Identification of biomarkers of brown adipose tissue aging highlights the role of dysfunctional energy and nucleotide metabolism pathways. *Scientific Reports*, *11*, 19928. https://doi.org/10.1038/s41598-021-99362-1

Marshall, A. G., Neikirk, K., Stephens, D. C., Vang, L., Vue, Z., Beasley, H. K., Crabtree, A., Scudese, E., Lopez, E. G., Shao, B., Krystofiak. E., Rutledge, S., Davis, J., Murray, S. A., Damo, S. M., Katti, P., & Hinton, A. Jr. (2023). Serial block face-Scanning electron microscopy as a burgeoning technology. *Advanced Biology (Weinh)*, *7*(8), e2300139. https://doi.org/10.1002/adbi.202300139

Nadal-Casellas, A., Bauzá-Thorbrügge, M., Proenza, A. M., Gianotti, M., & Lladó, I. (2013). Sex-dependent differences in rat brown adipose tissue mitochondrial biogenesis and insulin signaling parameters in response to an obesogenic diet. *Molecular and Cellular Biochemistry*, *373*, 125–135. https://doi.org/10.1007/s11010-012-1481-x

Naik, P. P., Praharaj, P. P., Bhol, C. S., Panigrahi, D. P., Mahapatra, K. K., Patra, S., Saha, S., & Bhutia, S. K. (2019). Mitochondrial heterogeneity in stem cells. In A. Birbrair (Ed.), *Stem cells heterogeneity—novel concepts* (pp. 179–194). Advances in Experimental Medicine and Biology. Springer International Publishing. https://doi.org/10.1007/978-3-030-11096-3_11

Neikirk, K., Lopez, E.-G., Marshall, A. G., Alghanem, A., Krystofiak, E., Kula, B., Smith, N., Shao, J., Katti, P., & Hinton, A. O. (2023). Call to action to properly utilize electron microscopy to measure organelles to monitor disease. *European Journal of Cell Biology*, *102*, 151365. https://doi.org/10.1016/j.ejcb.2023.151365

Neikirk, K., Vue, Z., Katti, P., Rodriguez, B. I., Omer, S., Shao, J., Christensen, T., Garza Lopez, E., Marshall, A., Palavicino-Maggio, C. B., Ponce, J., Alghanem, A. F., Vang, L., Barongan, T., Beasley, H. K., Rodman, T., Stephens, D., Mungai, M., Correia, M., Exil, V., … Hinton, A. O. Jr. (2023). Systematic transmission electron microscopy-based identification and 3D reconstruction of cellular degradation machinery. *Advanced Biology*, *7*, 2200221. https://doi.org/10.1002/adbi.202200221

Nirengi, S., & Stanford, K. (2023). Brown adipose tissue and aging: A potential role for exercise. *Experimental Gerontology*, *178*, 112218. https://doi.org/10.1016/j.exger.2023.112218

Pereira, R. O., Olvera, A. C., Marti, A., Fang, S., White, J. R., Westphal, M., Hewezi, R., AshShareef, S. T., García-Peña, L. M., Koneru, J., Potthoff, M. J., & Abel, E. D. (2022). OPA1 regulates lipid metabolism and cold-induced browning of White adipose tissue in mice. *Diabetes*, *71*, 2572–2583. https://doi.org/10.2337/db22-0450

Peres Valgas da Silva, C., Shettigar, V. K., Baer, L. A., Abay, E., Madaris, K. L., Mehling, M. R., Hernandez-Saavedra, D., Pinckard, K. M., Seculov, N. P., Ziolo, M. T., & Stanford, K. I. (2022). Brown adipose tissue prevents glucose intolerance and cardiac remodeling in high-fat-fed mice after a mild myocardial

infarction. *International Journal of Obesity*, *46*, 350–358. https://doi.org/10.1038/s41366-021-00999-9

Pfannenberg, C., Werner, M. K., Ripkens, S., Stef, I., Deckert, A., Schmadl, M., Reimold, M., Häring, H.-U., Claussen, C. D., & Stefan, N. (2010). Impact of age on the relationships of brown adipose tissue with sex and adiposity in humans. *Diabetes*, *59*, 1789–1793. https://doi.org/10.2337/db10-0004

Renne, M. F., & Hariri, H. (2021). Lipid droplet-organelle contact sites as hubs for fatty acid metabolism, trafficking, and metabolic channeling. *Frontiers in Cell and Developmental Biology*, *9*, 726261. https://www.frontiersin.org/articles/10.3389/fcell.2021.726261

Rodríguez-Cuenca, S., Pujol, E., Justo, R., Frontera, M., Oliver, J., Gianotti, M., & Roca, P. (2002). Sex-dependent thermogenesis, differences in mitochondrial morphology and function, and adrenergic response in brown adipose tissue. *Journal of Biological Chemistry*, *277*, 42958–42963. https://doi.org/10.1074/jbc.M207229200

Rovira-Llopis, S., Bañuls, C., Diaz-Morales, N., Hernandez-Mijares, A., Rocha, M., & Victor, V. M. (2017). Mitochondrial dynamics in type 2 diabetes: Pathophysiological implications. *Redox Biology*, *11*, 637–645. https://doi.org/10.1016/j.redox.2017.01.013

Samuelson, I., & Vidal-Puig, A. (2020). Studying brown adipose tissue in a human in vitro context. *Frontiers in Endocrinology*, *11*, 629. https://www.frontiersin.org/articles/10.3389/fendo.2020.00629

Sellayah, D., & Sikder, D. (2014). Orexin restores aging-related brown adipose tissue dysfunction in male mice. *Endocrinology*, *155*, 485–501. https://doi.org/10.1210/en.2013-1629

Song, A., Dai, W., Jang, M. J., Medrano, L., Li, Z., Zhao, H., Shao, M., Tan, J., Li, A., Ning, T., et al. (2020). Low- and high-thermogenic brown adipocyte subpopulations coexist in murine adipose tissue. *Journal of Clinical Investigation*, *130*, 247–257. https://doi.org/10.1172/JCI129167

Song, Y.-F., Hogstrand, C., Ling, S.-C., Chen, G.-H., & Luo, Z. (2020). Creb-Pgc1α pathway modulates the interaction between lipid droplets and mitochondria and influences high fat diet-induced changes of lipid metabolism in the liver and isolated hepatocytes of yellow catfish. *The Journal of Nutritional Biochemistry*, *80*, 108364. https://doi.org/10.1016/j.jnutbio.2020.108364

Tajima, K., Ikeda, K., Chang, H.-Y., Chang, C.-H., Yoneshiro, T., Oguri, Y., Jun, H., Wu, J., Ishihama, Y., & Kajimura, S. (2019). Mitochondrial lipoylation integrates age-associated decline in brown fat thermogenesis. *Nature Metabolism*, *1*, 886–898. https://doi.org/10.1038/s42255-019-0106-z

Tarnopolsky, M. A., Rennie, C. D., Robertshaw, H. A., Fedak-Tarnopolsky, S. N., Devries, M. C., & Hamadeh, M. J. (2007). Influence of endurance exercise training and sex on intramyocellular lipid and mitochondrial ultrastructure, substrate use, and mitochondrial enzyme activity. *American Journal of Physiology-Regulatory, Integrative and Comparative Physiology*, *292*, R1271–R1278. https://doi.org/10.1152/ajpregu.00472.2006

Tilokani, L., Nagashima, S., Paupe, V., & Prudent, J. (2018). Mitochondrial dynamics: Overview of molecular mechanisms. *Essays in Biochemistry*, *62*, 341–360. https://doi.org/10.1042/EBC20170104

Townsend, K. L., & Tseng, Y.-H. (2014). Brown fat fuel utilization and thermogenesis. *Trends in Endocrinology & Metabolism*, *25*, 168–177. https://doi.org/10.1016/j.tem.2013.12.004

Velickovic, K., Wayne, D., Leija, H. A. L., Bloor, I., Morris, D. E., Law, J., Budge, H., Sacks, H., Symonds, M. E., & Sottile, V. (2019). Caffeine exposure induces browning features in adipose tissue in vitro and in vivo. *Scientific Reports*, *9*, 9104. https://doi.org/10.1038/s41598-019-45540-1

Vincent, A. E., White, K., Davey, T., Philips, J., Ogden, R. T., Lawless, C., Warren, C., Hall, M. G., Ng, Y. S., Falkous, G., Holden, T., Deehan, D., Taylor, R. W., Turnbull, D. M., & Picard, M. (2019). Quantitative 3D mapping of the human skeletal muscle mitochondrial network. *Cell Reports*, *26*, 996–1009.e4. https://doi.org/10.1016/j.celrep.2019.01.010

Vue, Z., Garza-Lopez, E., Neikirk, K., Katti, P., Vang, L., Beasley, H., Shao, J., Marshall, A. G., Crabtree, A., Murphy, A. C., Jenkins, B. C., Prasad, P., Evans, C., Taylor, B., Mungai, M., Killion, M., Stephens, D., Christensen, T. A., Lam, J., … Hinton, A. Jr. (2023). 3D reconstruction of murine mitochondria reveals changes in structure during aging linked to the MICOS complex. *Aging Cell*, *22*(12), e14009. https://doi.org/10.1111/acel.14009

Vue, Z., Neikirk, K., Vang, L., Garza-Lopez, E., Christensen, T. A., Shao, J., Lam, J., Beasley, H. K., Marshall, A. G., Crabtree, A., Anudokem, J., Rodriguez, B., Kirk, B., Bacevac, S., Barongan, T., Shao, B., Stephens, D. C., Kabugi, K., Koh, H. J., … Hinton, A. (2023). Three-dimensional mitochondria reconstructions of murine cardiac muscle changes in size across aging. *American Journal of Physiology-Heart and Circulatory Physiology*, *325*, H965–H982. https://doi.org/10.1152/ajpheart.00202.2023

Wikstrom, J. D., Mahdaviani, K., Liesa, M., Sereda, S. B., Si, Y., Las, G., Twig, G., Petrovic, N., Zingaretti, C., Graham, A., Cinti, S., Corkey, B. E., Cannon, B., Nedergaard, J., & Shirihai, O. S. (2014). Hormone-induced mitochondrial fission is utilized by brown adipocytes as an amplification pathway for energy expenditure. *The EMBO Journal*, *33*, 418–436. https://doi.org/10.1002/embj.201385014

Yang, M., Luo, S., Yang, J., Chen, W., He, L., Liu, D., Zhao, L., & Wang, X. (2022). Lipid droplet–mitochondria coupling: A novel lipid metabolism regulatory hub in diabetic nephropathy. *Front Endocrinol (Lausanne)*, *13*, 1017387. https://doi.org/10.3389/fendo.2022.1017387

Yu, J., Zhang, S., Cui, L., Wang, W., Na, H., Zhu, X., Li, L., Xu, G., Yang, F., Christian, M., & Liu, P. (2015). Lipid droplet remodeling and interaction with mitochondria in mouse brown adipose tissue during cold treatment. *Biochimica et Biophysica Acta (BBA) - Molecular Cell Research*, *1853*, 918–928. https://doi.org/10.1016/j.bbamcr.2015.01.020

Zadoorian, A., Du, X., & Yang, H. (2023). Lipid droplet biogenesis and functions in health and disease. *Nature Reviews Endocrinology*, *19*, 443–459. https://doi.org/10.1038/s41574-023-00845-0

Zhou, X., Li, Z., Qi, M., Zhao, P., Duan, Y., Yang, G., & Yuan, L. (2020). Brown adipose tissue-derived exosomes mitigate the metabolic syndrome in high fat diet mice. *Theranostics*, *10*, 8197–8210. https://doi.org/10.7150/thno.43968

SUPPORTING INFORMATION

Additional supporting information can be found online in the Supporting Information section at the end of this article.

How to cite this article: Crabtree, A., Neikirk, K., Pinette, J. A., Whiteside, A., Shao, B., Bedenbaugh, J., Vue, Z., Vang, L., Le, H., Demirci, M., Ahmad, T., Owens, T. C., Oliver, A., Zeleke, F., Beasley, H. K., Lopez, E. G., Scudese, E., Rodman, T., Kabugi, K., … Hinton, A. (2024). Quantitative assessment of morphological changes in lipid droplets and lipid–mito interactions with aging in brown adipose. *Journal of Cellular Physiology*, *239*, e31340. https://doi.org/10.1002/jcp.31340